Shimming and MRSI

HP Hetherington and JW Pan, Yale University

INTRODUCTION

With the advent of high field 3T and ultrahigh field 7T MR systems, significant improvements in a variety of brain imaging modalities were anticipated. Although improvements in SNR have been demonstrated at 3T and 7T [1, 2], limitations due to increased static field (B_0) inhomogeneity have also been noted. One modality particularly affected by poor B_0 homogeneity is magnetic resonance spectroscopic imaging, (MRSI). Although excellent B_0 homogeneity is a requisite for MRSI, the hardware requirements in terms of shim strength and shim order necessary for 7T is controversial, with the majority of systems delivered having only 2nd order shims. The arguments forwarded against the efficacy of higher order shims include: 1) the required strengths for higher order terms are sufficiently large as to make them unattainable with conventional shim technology and 2) the effects of higher order terms across individual voxels is minimal due to the small voxel sizes used in MRSI studies. The first issue, which is characterized by the global homogeneity, $\sigma \mathbf{B}_0^{\text{Global}}$, and calculated over the entire ROI is a significant factor in determining the performance of frequency selective pulses, such as those generally used for water suppression or spectral editing. The second issue is characterized by the local homogeneity, $\sigma \mathbf{B}_0^{\text{Local}}$, which is measured over individual voxels and impacts spectral resolution within a voxel. This latter effect can significantly impact the number of pixels which provide useable spectra. Therefore, in this presentation we will: 1) evaluate the role and requirements for 3rd order shims for SI studies at 7T for both $\sigma \mathbf{B}_0^{\text{Global}}$ and $\sigma \mathbf{B}_0^{\text{Local}}$; 2) demonstrate high resolution spectroscopic imaging from a variety of brain regions using 1st-3rd order shimming and 3) evaluate the potential role for 4th order shimming.

METHODS

To evaluate the regional requirements for single slice MRSI studies, data from 60 subjects (20 for each brain region) was acquired using single slice studies from three representative brain regions: 1) the frontal lobes at the level of the supplementary motor area (SMA), 2) the parietal lobe at the level of the thalamus and basal ganglia (subcortical nuclei - SCN), and 3) the temporal lobe at the level of the hippocampus (MTL). All data were acquired with a Varian Direct Drive system and a head only (68cm ID) actively shielded 7T magnet. The gradient system (Varian Inc.) included a full set of 2nd and 3rd order shims, with each shim driven by two 10A shim power supplies (Resonance Research Inc.). A non-iterative multi-slice B_0 mapping method was used to acquire B_0 maps, calculate necessary shim currents and to set all 1st-3rd order terms [3]. Following adjustment of the shims, a second B_0 map was acquired to document the improvement in $\sigma \mathbf{B}_0^{\text{Global}}$ over the target ROIs. As part of the optimization, a predicted residual standard deviation after applying the shim currents was calculated. The predicted and measured standard deviation of the B_0 field over the target ROI ($\sigma \mathbf{B}_0^{\text{Global}}$) varied by less than 1Hz for a single pass. We also calculated the requirements and potential improvement for the inclusion of 4th order corrections. For calculations involving 4th order shims, the maximal values for 4th order terms were not constrained; however all lower order terms were constrained by the existing hardware limits.

To determine the effect of shimming over an “SI pixel” the ROI selected for shimming was divided into an array of ~1cc volumes consisting of 3x3x3 B_0 map pixels each. The standard deviation of the B_0 field across each 1cc sub-volume, $\sigma \mathbf{B_0}^{\text{local}}$, was then calculated and

pooled across all subjects for a given location. Spectroscopic imaging data was acquired using a short TE (15ms) sequence [4, 5]. Phase encoding was performed using a rectangular sampling scheme (24x24 encodes) over a FOV of 192x192mm^2 achieving a nominal voxel of 0.64cc (~1cc after filtering). The TR was 1.5s resulting in acquisition times of 14.4minutes.

RESULTS: σB_0^{Global}

Displayed in Fig. 1 are B_0 maps acquired from the three regions of interest prior to shimming and after adjustment of all first-third order terms. To evaluate the extent to which each shim order provides improvement, we pooled values of σB_0^{Global} obtained using 1st, 1st&2nd and 1st-3rd order shims for the three regions from the 20 volunteers in each group (Fig 2). In this case significant improvements, reductions of 26, 29 and 37% in σB_0^{Global} were obtained when third order shims were added to 1st and 2nd order terms for the three locations. Notably a significant improvement was achieved even for most superior slice when third order shims were added. None of the 2nd-3rd order values used exceeded more than 39% of the available shim strength in any subject, indicating that correction of third order inhomogeneities was possible with the existing hardware configuration.

Figure 1: Representative Maps of σB_0^{Global}

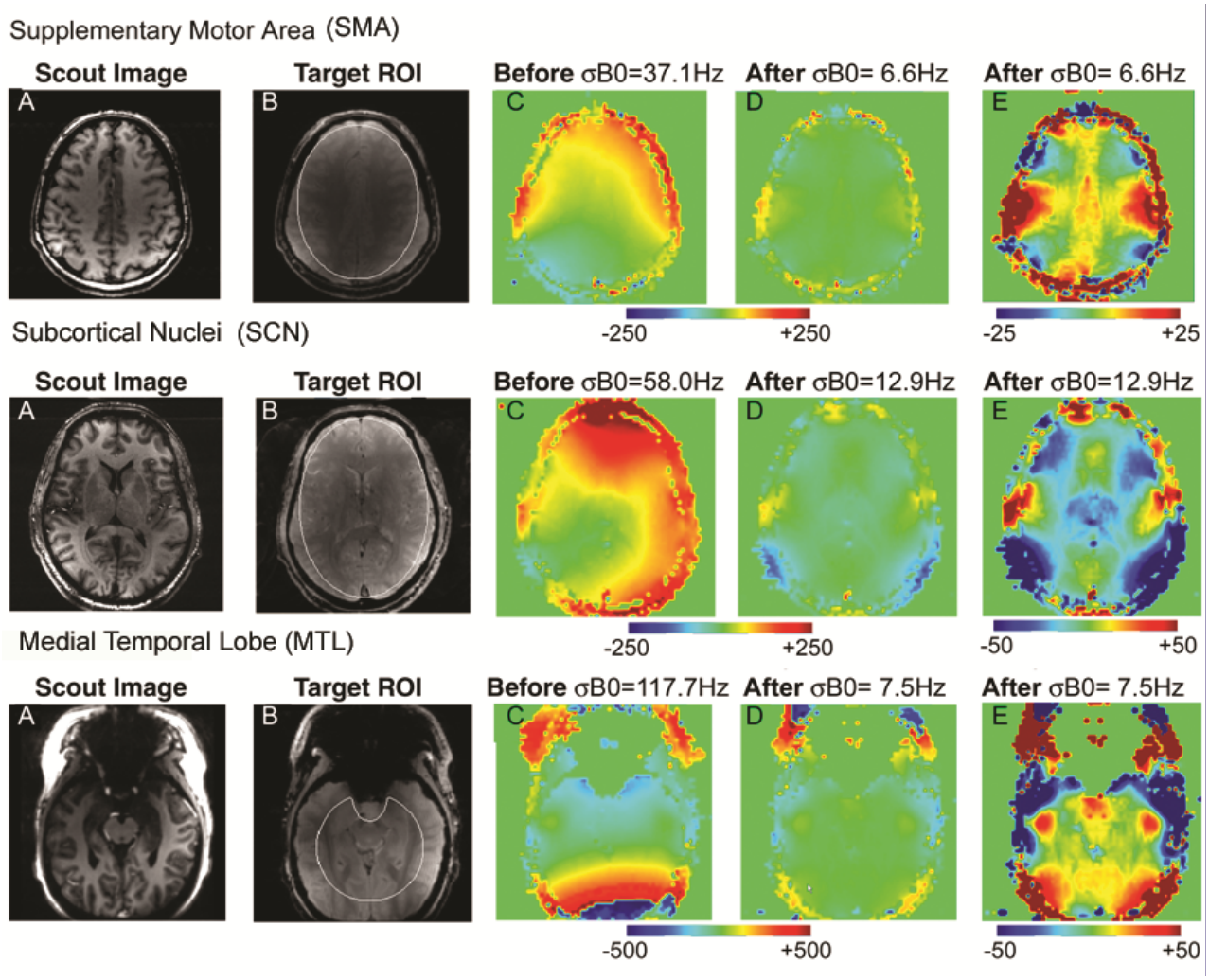

Figure 2: Pooled data of σB_0^{Global}

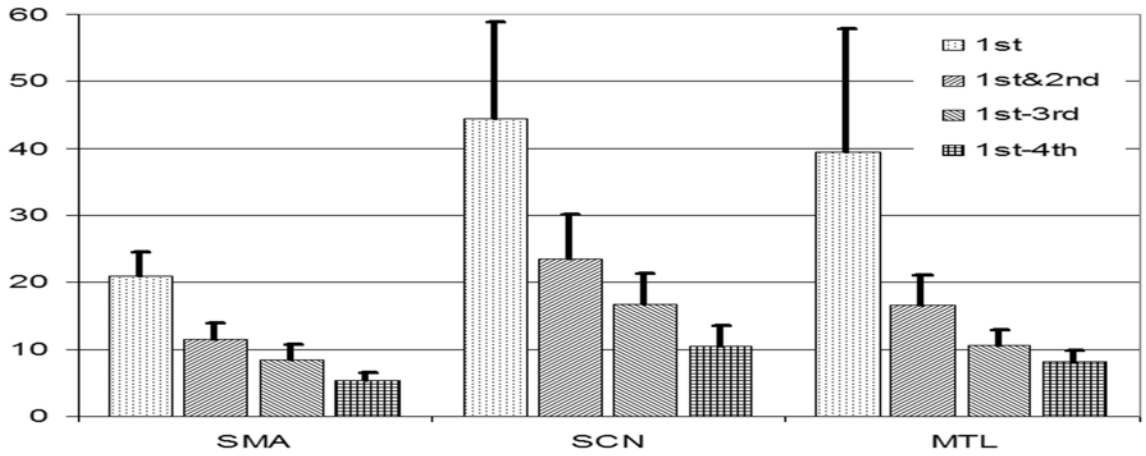

To assess the extent to which corrections for fourth order terms could improve the overall homogeneity, we calculated the residual σB_0^{Global} including all first through fourth order terms for all three locations. In this simulation, the 1^{st}-3^{rd} orders are constrained by the limitations of our current hardware and 4^{th} order shims are not. When all fourth order terms were included, σB_0^{Global} decreased from 8.5, 16.7 and 10.5 Hz to 5.3, 10.5, and 8.1 Hz for the three slices (SMA, SCN and MTL respectively). In this case the fractional improvement in overall homogeneity was 38, 37 and 23% percent respectively.

Results : σB_0^{Local}

To evaluate the role of higher order shimming on σB_0^{Local} we calculated σB_0^{Local} for each "SI pixel" in the ROI and pooled the data across all volunteers. The data was binned in increments of 0.25Hz. Displayed in Fig. 3a-c are the normalized distributions of the values measured for σB_0^{Local} for the three regions using progressively higher order shimming. To better visualize the impact of having higher order shims on σB_0^{Local} we have also plotted the data as a function of the fraction of "SI pixels" achieving a given σB_0^{Local} (Fig 4a-c). Depending upon the σB_0^{Local} required the fraction of useable pixels in the ROI for a given slice and shim order can be estimated. For each successive shim order, the curve shifts to the left, indicating a larger number of pixels achieving a given σB_0^{Local}. In this case, improvements are seen for not only for the addition of 3^{rd} order shims but also fourth order terms.

Figure 3: Histograms of σB_0^{Local}

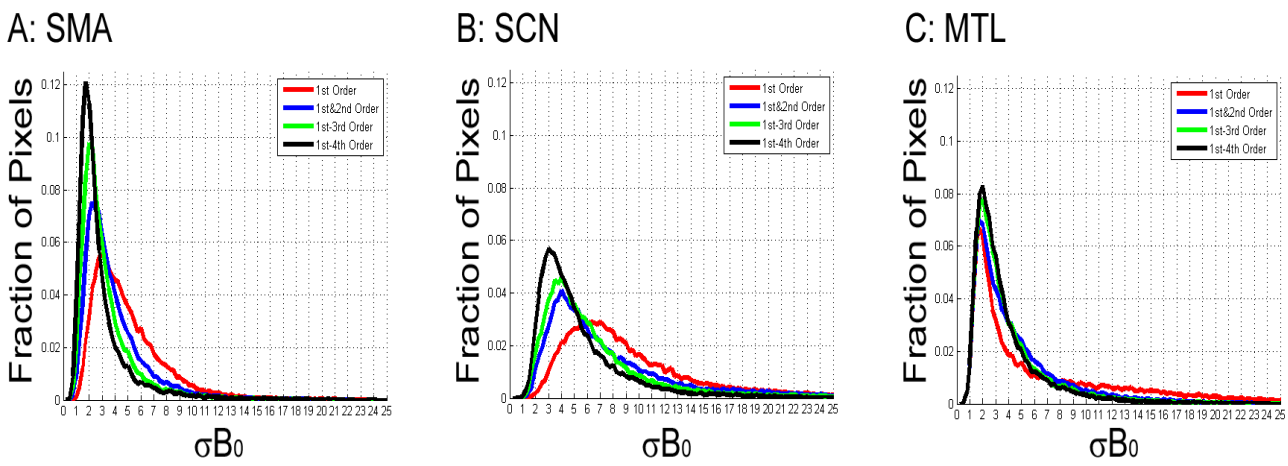

Figure 4: Cumulative Histograms of σB_0^{Local}

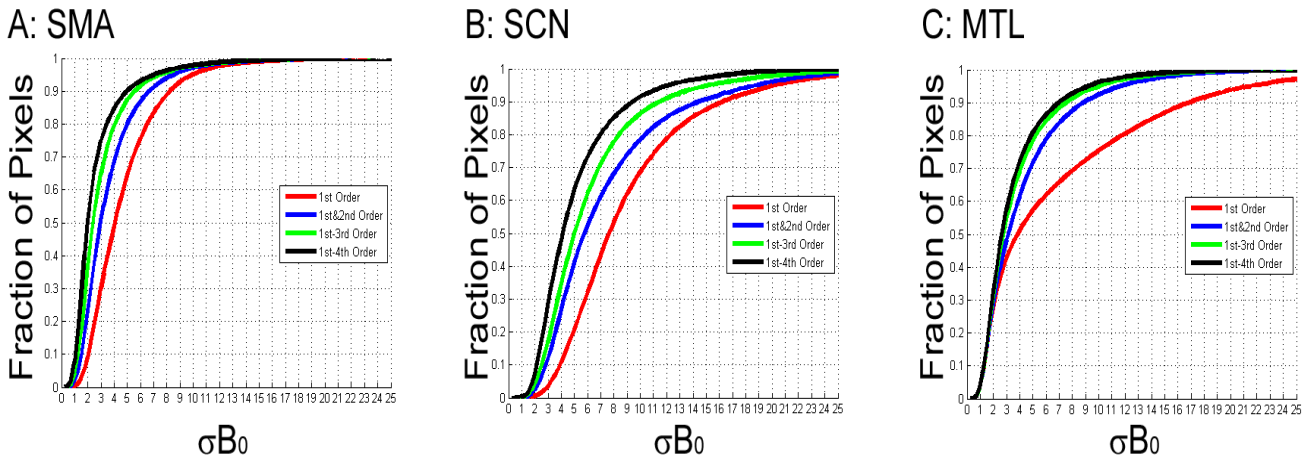

Results: MRSI

Displayed in Figures 5-7 are spectroscopic imaging data acquired using 1^{st}-3^{rd} order shims for the three slices. In each figure maps of σB_0^{Local} attained using 1^{st}&2^{nd} order shimming, 1^{st}-3^{rd} order shimming and that calculated for 1^{st}-4^{th} order shimming are presented along with representative spectra. Consistent with the pooled data shown in Figs 3 and 4, addition of third order shimming improves σB_0^{Local} for the SMA slice (Fig.5). The addition of third order shims has the largest effect in improving the σB_0^{Local} of voxels over the cortical periphery. Addition of 4^{th} order shims of sufficient strength are predicted to further improve the peripheral cortical regions resulting a highly homogeneous distribution of σB_0^{Local} across the entire slice. In data acquired with third order shims, the substantial increase in glutamate and creatine from gray matter (5a-d) is easily seen in comparison to white matter (5e-h).

Figure 5: Spectroscopic Imaging of SMA and σB_0^{Local}

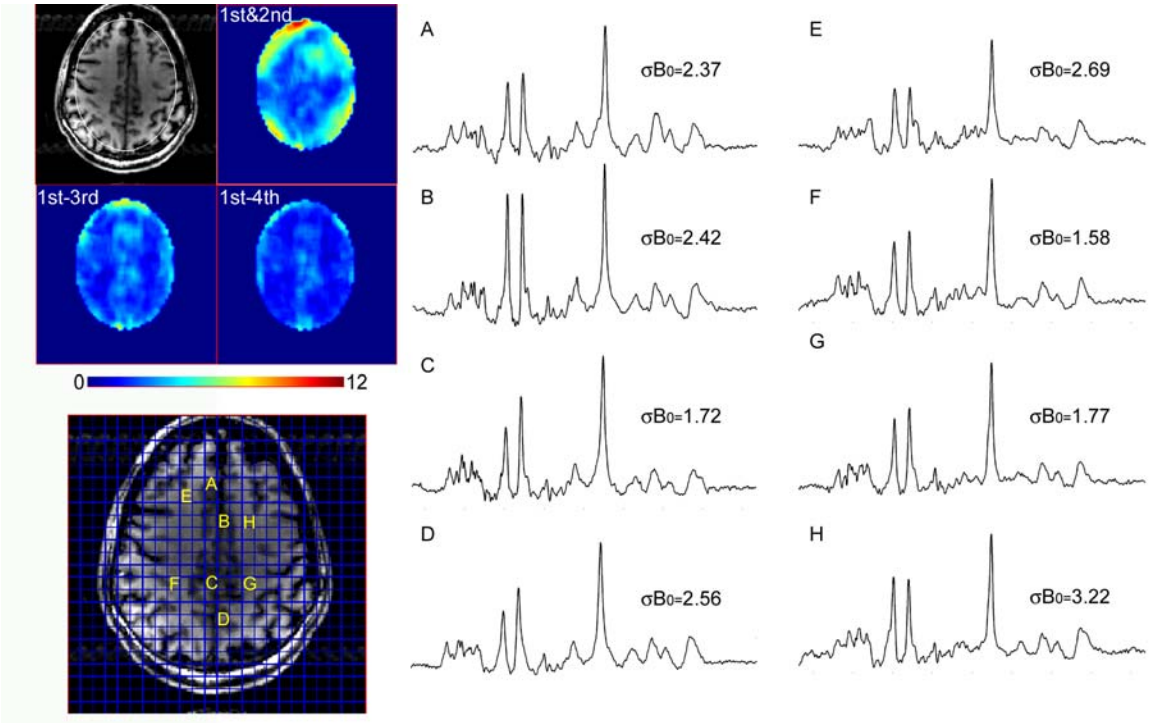

For the SCN slice containing the thalamus and basal ganglia, as expected σB_0^{Local} is markedly higher in comparison to the SMA slice. In addition to poorer homogeneity over the cortical periphery, a large susceptibility artifact superior to the frontal sinuses, over the anterior horns of the ventricles is seen for 2nd order shimming which merges with the frontal cortical periphery. Addition of third order shimming reduces both the inhomogeneity over the cortical periphery and regions lateral and anterior the artifact from the frontal sinuses. For well shimmed regions such as the thalamus (6a), posterior brain locations (6b, c) and the insula (6d, e), σB_0^{Local} <4Hz, excellent spectral resolution is achieved. Despite the relatively small size of the voxels (~1cc), substantial spectral quality degradation is seen on a pixel by pixel basis as one approaches the anterior horns of the ventricles (Fig. 6e-h). As expected, based on the maps of σB_0^{Global}, addition of 4th order shims with sufficient strength significantly reduces both the extent and severity of inhomogeneity from this brain region and peripheral cortical regions.

Figure 6: Spectroscopic Imaging of SCN and σB_0^{Local}

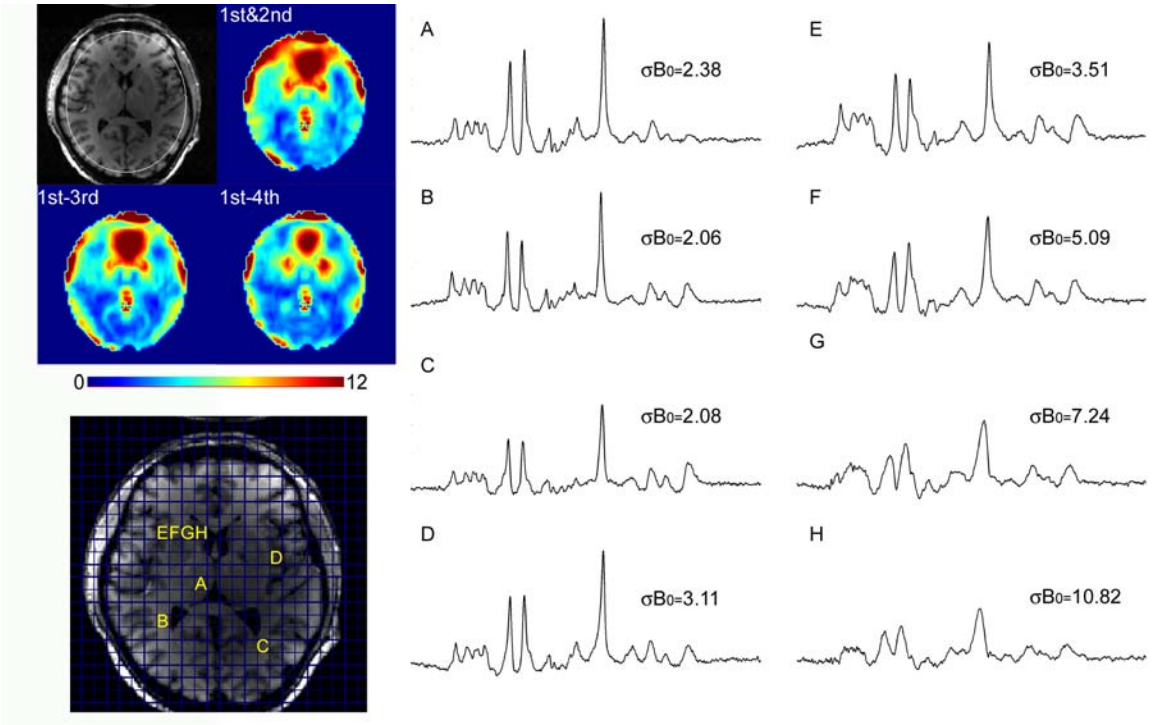

For the MTL slice, despite the small size of the target ROI, the majority of the anterior region displays σB_0^{Local}>12Hz when only 2nd order shimming is available. Additionally for this subject, relatively poor homogeneity σB_0^{Local} >12Hz is also seen from the posterior portion of the ROI. Addition of 3rd order shimming dramatically improves the homogeneity over the entire ROI enabling nearly the entire posterior region of the ROI to achieve σB_0^{Local} <6Hz. additionally, the poor homogeneity regions (σB_0^{Local} >12Hz) over adjacent to the frontal sinus are substantially decreased in extent and severity. As displayed in Fig 7a-j, although σB_0^{Local} degrades as one moves along the hippocampal formation in the anterior direction, even the most anterior pixels yield sufficient resolution to identify major singlets such as NAA, creatine and choline when third order shimming is used. Unlike the SMA and SCN, the predicted improvements in σB_0^{Local} with fourth order shimming are more modest, primarily reflecting improvements in the posterior portion of the ROI and small improvements in the anterior regions. This modest predicted

improvement largely reflects the existence of a significant fifth order inhomogeneity term in this region.

Figure 7: Spectroscopic Imaging of MTL and σB_0^{Local}

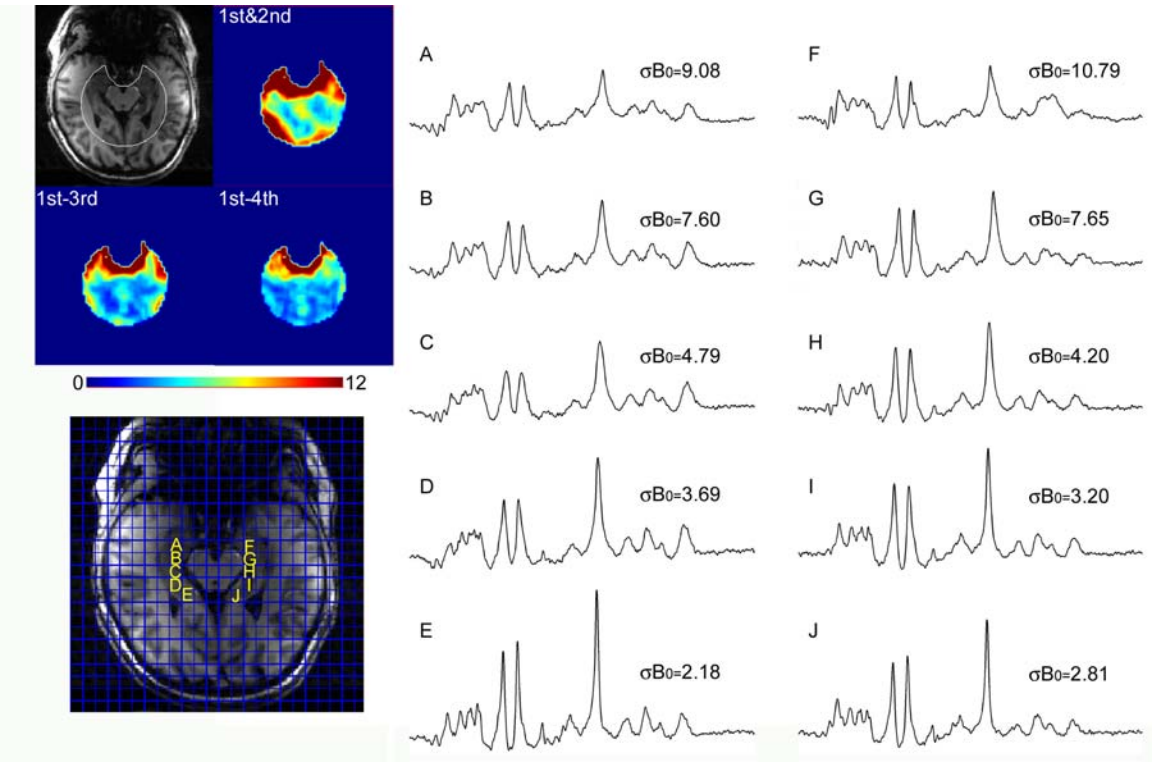

CONCLUSIONS

As demonstrated, higher order shimming can have a significant impact on both overall homogeneity, σB_0^{Global}, and local homogeneity, σB_0^{Local}, even when small SI voxels are used (<1cc). For third order shimming, sufficient strength can be generated with existing technologies to provide substantial improvements over 2nd order shimming for spectroscopic imaging studies. Use of even higher order shimming has the potential to significantly improve both σB_0^{Global} and σB_0^{Local} for spectroscopic imaging applications if sufficient strength can be achieved.

REFERENCES

1. Vaughan, J.T., et al., *7T vs. 4T: RF power, homogeneity, and signal-to-noise comparison in head images.* Magn Reson Med, 2001. **46**(1): p. 24-30.
2. Gonen, O., et al., *Proton MR spectroscopic imaging of rhesus macaque brain in vivo at 7T.* Magn Reson Med, 2008. **59**(4): p. 692-9.
3. Hetherington, H.P., et al., *Robust fully automated shimming of the human brain for high-field 1H spectroscopic imaging.* Magn Reson Med, 2006. **56**(1): p. 26-33.
4. Avdievich, N.I., et al., *Short echo spectroscopic imaging of the human brain at 7T using transceiver arrays.* Magn Reson Med, 2009.
5. Hetherington, H.P., et al., *RF shimming for spectroscopic localization in the human brain at 7 T.* Magn Reson Med, 2009.